WARWICK
THE UNIVERSITY OF WARWICK

Manuscript version: Author's Accepted Manuscript
The version presented in WRAP is the author's accepted manuscript and may differ from the published version or Version of Record.

Persistent WRAP URL:
http://wrap.warwick.ac.uk/151070

How to cite:
Please refer to published version for the most recent bibliographic citation information. If a published version is known of, the repository item page linked to above, will contain details on accessing it.

Copyright and reuse:
The Warwick Research Archive Portal (WRAP) makes this work by researchers of the University of Warwick available open access under the following conditions.

© 2021 Elsevier. Licensed under the Creative Commons Attribution-NonCommercial-NoDerivatives 4.0 International http://creativecommons.org/licenses/by-nc-nd/4.0/.

Publisher's statement:
Please refer to the repository item page, publisher's statement section, for further information.

For more information, please contact the WRAP Team at: wrap@warwick.ac.uk.

warwick.ac.uk/lib-publications

Moment-less Arches for Reduced Stress State. Comparisons with Conventional Arch Forms.

W. J. Lewis*[a], J. M. Russell[a]

[a]School of Engineering, University of Warwick, Coventry CV4 7AL

[b]T. Q. Li, Arup, London

Abstract

This paper presents a study of two-pin arches of constant cross-section that are moment-less under statistically prevalent (permanent) load. The arches are defined by analytical form-finding previously reported in [1]. The work provides guidance regarding the solution process, and expressions for reactions and axial forces. New analytical results include the derivation of the arch length, and a method for finding co-ordinates of individual arch segments in pre-fabricated construction. The accuracy of the shape prediction for inextensible moment-less arches is good, compared to the results from elastic models. Case studies report on medium and large-span arches, with the latter resembling the iconic Hoover Dam arch. Comparative studies of the moment-less and conventional arch forms (mostly of parabolic configuration), are carried out using permanent and variable loads. Additionally, the Hoover Dam arch is analysed for a discrete load transfer from the deck. Circular arches are analysed for the permanent load only, and are shown to be extremely inefficient in load resistance. Moment-less arches are found to provide a minimal stress response to loading and require least amount of material – a feature observed in natural objects. These characteristics are important from a durability perspective – a key concern for our future infrastructure.

Keywords: moment-less arches, funicular arches, analytical form-finding, parabolic arches, circular arch forms, Hoover Dam Bridge

Corresponding author: W.J. Lewis, w.j.lewis@warwick.ac.uk, School of Engineering, University of Warwick, Coventry CV4 7AL UK

1. Introduction

Climate change is producing unexpected environmental loads and has brought calls for more durable and sustainable design solutions. In view of this, it is necessary to re-examine the current design philosophy, which relies on stressing structures to a safe maximum limit, in order to secure efficient material usage. In doing so, the overall structural configuration, known to be responsible for stress variations, is not usually considered; this has an effect on the durability of a given structure. Discussed here are 2-pin arches of constant cross-section, subjected to permanent and variable loads. The main focus of the study are moment-less arch forms defined by analytical form-finding presented in [1]. These structures are unique, because they are shaped by a methodology that limits their stress response to loading, by allowing only compressive forces to develop under statistically prevalent load. It is assumed here that this is the permanent load, and as such, it has been chosen to define profiles of moment-less arches, allowing them to work in their optimal state of reduced stress most of the time. The complete design has to involve checks for variable load including permanent and transient loads, and this aspect has been considered in the paper.

Although some awareness of material and structural inefficiencies of conventional arch forms exists, especially in relation to circular arches, parabolic forms continue to be the norm in conceptual design of these structures. The aim of this work is to demonstrate the advantages of moment-less arches over conventional forms, particularly those of parabolic configuration. This work is intended to bring the theoretical concept of moment-less arches closer to practical application.

2. Past work

Timoshenko and Young [2] have long advocated the concept of moment-less arches in designing optimal structural forms, but the idea has not been embraced universally, and this is particularly noticeable in the education sector, which produces textbooks presenting detailed analyses of conventional arch forms [3]. There exists a substantial amount of literature on the topic of optimal arches modelled by a variety of computational/optimisation algorithms [4]. In many cases, it is assumed that the arch is weightless and the stress in them is generated just by the deck weight. Some researchers embraced the concept of an inverted hanging chain analogy, dating back to Robert Hooke [5], when shaping an optimal arch configuration. Reference [6] gives a ‘shape’ equation describing a chain of constant cross-section hanging under its own weight, and points out that this equation also describes an upside-down geometry of a funicular arch. This ‘inverted hanging chain analogy’ can be easily demonstrated using a form-finding experiment, during which a change from tensile stress in the chain, to compressive one in the arch, takes place. However, such a transition may not involve a direct reversal of stresses without further deformations, because of material elasticity – a point discussed in Section 7 of this paper. Significant contributions in the application of experimental form-finding to arch structures have been made by Gaudi [7-8] who initiated long-term projects, such as the famous Sagrada Familia (now over 100 years old). Otto [9] engaged in a broad research programme into form-finding, aimed at modelling a variety of lightweight structures, which included domes and arches. When it was discovered

that Gaudi used inverted chain analogy in shaping his church spires, it was in Otto's laboratory that a model of Güel Colony church was built. The original project was not completed due to the Spanish Civil war, but a photograph that was recovered indicated that the elegant looking spires of the church were shaped by the weight of hanging chains and point loads exerted by small bags of sand attached to them. The form was that of a series of funicular arches. We can presume that Gaudi used the same design method when conceiving Sagrada Familia. Clearly, the load was well chosen, as the structure has withstood the test of time.

There are exists a substantial amount of literature dedicated to form-finding and optimisation of masonry arches. Its main focus is on achieving an acceptable shape of a thrust line that ensures pure compressive, rather than bending-free, actions [10, 11]. Typically, only the arch weight is considered, often in combination with the horizontal load, and the optimisation process leads to arches of varied cross-section. The requirement of pure compression is less severe than the bending-free action, advocated in this paper to ensure a more uniform compressive stress distribution across the arch cross-section. Another feature distinguishing the work from that proposed here is the use of transient, rather than statistically prevalent, load in shaping the arch. Arches of varied cross-section are outside the scope of this paper.

In the field of computational form-finding, spatial funicular arches deserve attention, with recent developments including the application of the Force Density method, previously used in shaping tensioned cable networks [12, 13]. While literature reporting on computational methods for optimising shapes of arch structures is substantial, work on analytical solutions for funicular arches of constant cross-section, and subjected to statistically prevalent load, such as the deck and arch weights, is almost non-existent. Other than reference [1], Wang and Wang [14] made a significant contribution to finding a solution for the centre-line profile of a funicular arch (cable), by making a different choice of parameter and following a different procedure to that in [1]. The work is elegant in its exposition and correctly identifies three possible solutions for the arch configuration, depending on the deck weight/arch weight ratio. However, the study stops short of producing the expression for the horizontal reaction, and the end limit for the chosen parameter, namely, the varying slope of the centre-line profile of the arch. Furthermore, the suggested graphical solution for finding the horizontal reaction would need to be interpreted algebraically, to yield the accuracy required in defining the arch centre-line profile.

3. Present work

In this paper, the results of the analytical form-finding theory defining moment-less arch forms in [1] are systematically analysed and developed to improve their suitability for practical application. A summary of the main features of the theory is given, together with a guidance regarding the solution process. The results based on the moment-less arch model that assumes the structure to be inextensible are compared with those of a linear elastic one from finite element analyses using GSA [15] and ABAQUS [16] software.

The work is supported by two groups of case studies. The first concerns a medium-span arch, with the deck weight/arch weight ratio, $r = 2$. The second is a large-span structure, resembling the iconic Hoover Dam bridge, with $r = 0.714$. New theoretical contributions presented here include the derivation of arch length and the end co-ordinates of funicular arch segments. These are directed at facilitating a pre-fabricated design/construction. The overall solution provides not only the arch geometry, but also the reactions and axial forces developing in the structure under permanent load. Finite element modelling using the aforementioned software is used to (i) test the assumption of inextensible behaviour of the moment-less arch, and (ii) to analyse the case of variable load comprising permanent and live (transient) load in the assessment of moment-less and parabolic arch forms. All computations required as part of the solution process, including the calculation for the length and segmental arch co-ordinates, reactions, and axial forces, have been carried out using Excel software.

4. Moment-less arch

4.1 Centre-line profile (ref [1])

The aim of the work reported in [1] was to find the centre-line profile of an arch subjected to statistically prevalent load, such as the permanent load. Figure 1 presents an idealised form of a rigid (inextensible) arch, carrying permanent load in the form of the arch weight, q, per arch length, and the deck weight, w, per unit span. Due to symmetry, only half of the arch is shown. The deck weight, w, can be applied either from above by using thin spandrel columns, or below, in the case of a deck suspended by cables. It is assumed that the series of point loads exerted by the elements transmitting the deck load to the arch can be treated as a uniformly distributed load, and the elements themselves are of negligible weight.

The theory makes use of a set of equilibrium equations, which initially describe bending, shear and axial compression of the arch. The imposition of zero shear - a necessary and sufficient condition for making the arch moment-less, renders the arch statically determinate. Consequently, vertical and horizontal reactions, as well as axial forces, can be found.

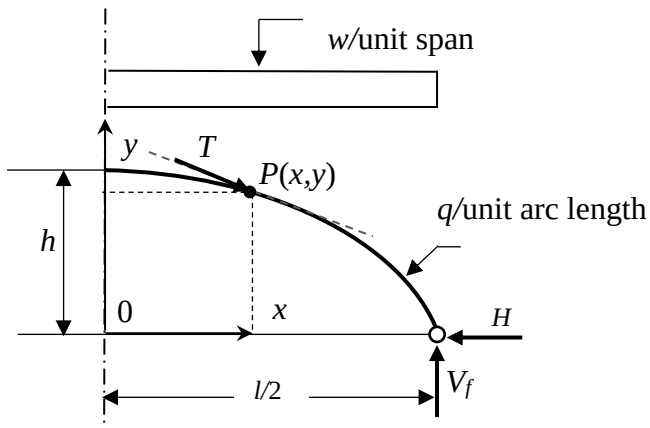

Figure 1. Idealised arch structure.

The equation for thrust, T, at any point P, given in [1] by:

$$T = \frac{1}{\left(1 + y'^2\right)^{1/2}} \left[H - y' \left(wx + q \int_0^{c(x)} ds \right) \right] \tag{4.1}$$

where y' is a derivative of y with respect to x, $c(x)$ is the length of the arch profile from the apex to an arbitrary point P, and ds is the differential arc length.

The parametric solution for the horizontal and vertical co-ordinates of the structure's centre-line profile is outlined below.

The solution for the y co-ordinates is given as:

$$y = h - \frac{1}{\beta}(z - 1) + \frac{r}{\beta} \ln \frac{r + z}{r + 1} \tag{4.2}$$

where $r = w/q$, $\beta = q/H$ and the parameter $z = \sqrt{1 + y'^2}$.

The parameter z takes values between 1 and $\bar{z}$; at $x = 0$, $z=1$, and at $x = l/2$, $z = \bar{z}$, where it is shown later that $\bar{z}$ can be determined from the end condition.

The solution for the x co-ordinates is given as:

$$x = \frac{1}{\beta} \cosh^{-1} z + \frac{1}{\beta} F(z) \tag{4.3}$$

where $F(z)$ depends on r, which creates three possible cases:

(a) $r > 1$, or $w > q$
(b) $r = 1$, or $w = q$
(c) $r < 1$, or $w < q$.

In case (a)

$$F(z) = -\frac{r}{\sqrt{r^2 - 1}} \ln \left[\frac{\sqrt{r + 1} + \sqrt{r - 1}}{\sqrt{r + 1} - \sqrt{r - 1}} \cdot \frac{z + \sqrt{z^2 - 1} + r - \sqrt{r^2 - 1}}{z + \sqrt{z^2 - 1} + r + \sqrt{r^2 - 1}} \right], \tag{4.3a}$$

in case (b)

$$F(z) = \frac{2}{z + \sqrt{z^2 - 1} + 1} - 1, \tag{4.3b}$$

in case (c)

$$F(z) = -\frac{2r}{\sqrt{1 - r^2}} \left[\mathrm{Tan}^{-1} \left(\frac{z + \sqrt{z^2 - 1} + r}{\sqrt{1 - r^2}} \right) - \mathrm{Tan}^{-1} \left(\frac{1 + r}{1 - r} \right)^{\frac{1}{2}} \right]. \tag{4.3c}$$

Using equation (4.2) and the boundary condition $y\,(l/2) = 0$, $z = \bar{z}$ gives:

$$h = \frac{1}{\beta}(\bar{z} - 1) - \frac{r}{\beta}\ln\frac{\bar{z} + r}{1 + r} \tag{4.4}$$

and substituting x = *l*/2 into equation (4.3) gives:

$$\frac{l}{2} = \frac{1}{\beta}cosh^{-1}\bar{z} + \frac{1}{\beta}F(\bar{z}). \tag{4.5}$$

Dividing equation (4.5) by (4.4) gives the required equation for $\bar{z}$, with β eliminated:

$$\frac{l}{2h} = \frac{\rho}{2} = \frac{\cosh^{-1}\bar{z} + F(\bar{z})}{\bar{z} - 1 - r\ln\frac{\bar{z} + r}{1 + r}}\ , \tag{4.6}$$

where $\rho = l/h$ is the span/rise ratio.

Once $\bar{z}$ is determined, β can be found from equation (4.4), or (4.5) and used to find the centre-line profile (eqns (4.2) and (4.3).

4.2 Arch length

A useful new addition to the solution given by eqns (4.2) to (4.6) is the derivation of the total length of the arch, *C*, measured along the centre-line profile. A detailed derivation is given in Appendix A, giving:

$$C = \frac{2}{\beta}\sqrt{(\bar{z}^2 - 1)} - rl. \tag{4.7}$$

It is found that the above formula is valid for all cases (a)-(c) described in Section 4.1, as shown in Appendix A.

4.3 End co-ordinates of arch segments

In pre-fabricated construction, it is helpful to know the co-ordinates defining the ends of individual segments from which the arch is to be built, with each segment comprising a number of discrete finite elements. With the arch length known, the lengths of individual segments can be easily calculated, but it is not straightforward to find the end co-ordinates of each segment, other than at the starting and end points of the arch. The methodology proposed below focuses on the segments of the moment-less arch, but can be adapted to conventional arches of, say, parabolic configuration.

If all segments are to be of equal length, then, from eqn. (4.7) the length of an individual segment, C_N, is:

$$C_N = \frac{C}{N}, \tag{4.8}$$

where *N* is the total number of equal length segments along the length of the arch. Then, the running lengths marking the ends of successive segments relative to the starting point are simply multiples of C_N.

In the case of varied length segments, the running lengths, C_n, marking the segmental end points, n, accumulate in a manner shown in (Fig. 2). Equation (4.7) gives the following relationship between C_n and x_n:

$$C_n = \frac{1}{\beta}\sqrt{{z_n}^2 - 1} - r x_n. \tag{4.9}$$

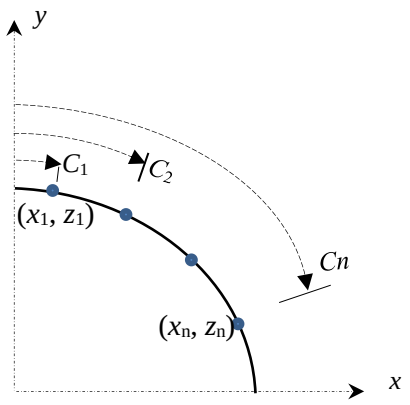

Figure 2. Lengths $\boldsymbol{C_n}$ marking segmental end points.

Equation (4.9) can be re-written to provide the following recurrence equation for two unknowns: x_n and z_n:

$${z_n}^i = \left[\beta^2\left(C_n + r{x_n}^i\right)^2 + 1\right]^{1/2}, \tag{4.10}$$

In which β is known/determined from eqn (4.4) or (4.5), C_n is found from the total arch length and chosen number of segments, r is a known input parameter, and i - an iterative step.

To start iterations, an initial estimate for ${x_n}^i$ can be taken from the co-ordinates describing the centre-line profile of the arch, as demonstrated in Case study 1 in Section 5.1) Once ${z^i}_n$ is found from equation (4.10), the co-ordinate ${x_n}^{i+1}$ can be found from eqn. (4.3) and used again in eqn (4.10). The iterative process continues until the difference in x_n between two successive iterations is small. The final value for z determines the x and y co-ordinates of the segmental end (eqns (4.3) and (4.2)). The iterative process is illustrated in Fig. 3.

4.4 Reactions and axial forces

As noted in Section 4.1, the horizontal reaction, H, can be found from $\beta = q/H$, giving:

$$H = \frac{q}{\beta}, \tag{4.11}$$

with β found from eqn (4.4) or (4.5), after $\bar{z}$ has been determined from eqn (4.6).

The vertical reaction, V_f, can be found by halving the total deck load and the arch weight:

$$V_f = \frac{w \cdot l + q \cdot C}{2}, \tag{4.12}$$

where C is found from eqn (4.7).

With $z = \sqrt{1 + y'^2}$, and y' being negative, the axial forces given by eqn (4.1) can written as:

$$T = \frac{1}{z}\left[H + \sqrt{z^2 - 1}\,(wx + qC_n)\right], \tag{4.13}$$

where C_n is given by eqn (4.9).

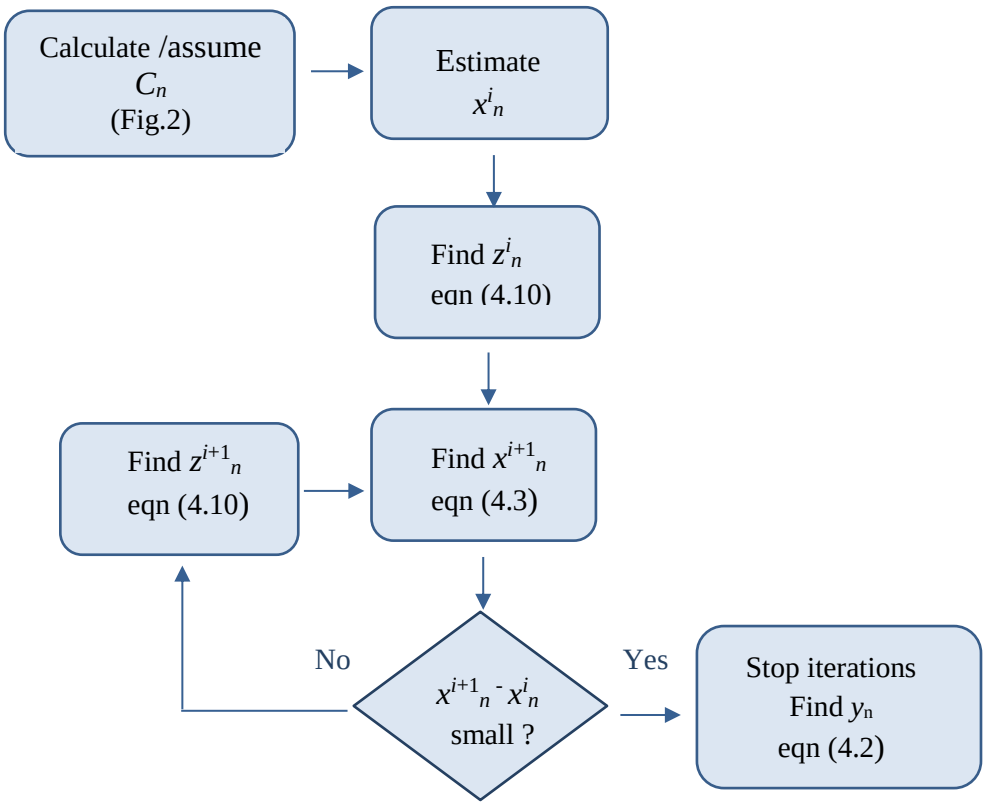

Figure 3. Iterative process of finding segmental end co-ordinates.

4.5 Overall solution procedure

The overall solution procedure of finding the centre-line profile of the moment-less arch, its reactions, axial forces, the arch length, and co-ordinates of arch segments, is illustrated by the flowchart in Fig. 4.

The process starts with finding $\bar{z}$ by solving eqn (4.6) numerically, for a given span/rise ratio, ρ, and ratio of loading, r. In any iterative solution, a plausible initial value for $\bar{z}$ is that for the parabolic case, viz., $\bar{z}_{initial} = (1 + 16/\rho^2)^{1/2}$. The solution can be obtained using a number of simple numerical algorithms. The accuracy of the $\bar{z}$ can be checked by calculating the x and y co-ordinates; if x does not close at the correct value at the end of the span, further iterations are needed to find a more accurate solution.

The key parameters of the overall solution are $\bar{z}$ and β; they determine not only the arch centre-line profile, but also the horizontal reaction, H. To facilitate the design process, it is possible to generate a database of $\bar{z}$ and β to cover a majority of practical situations.

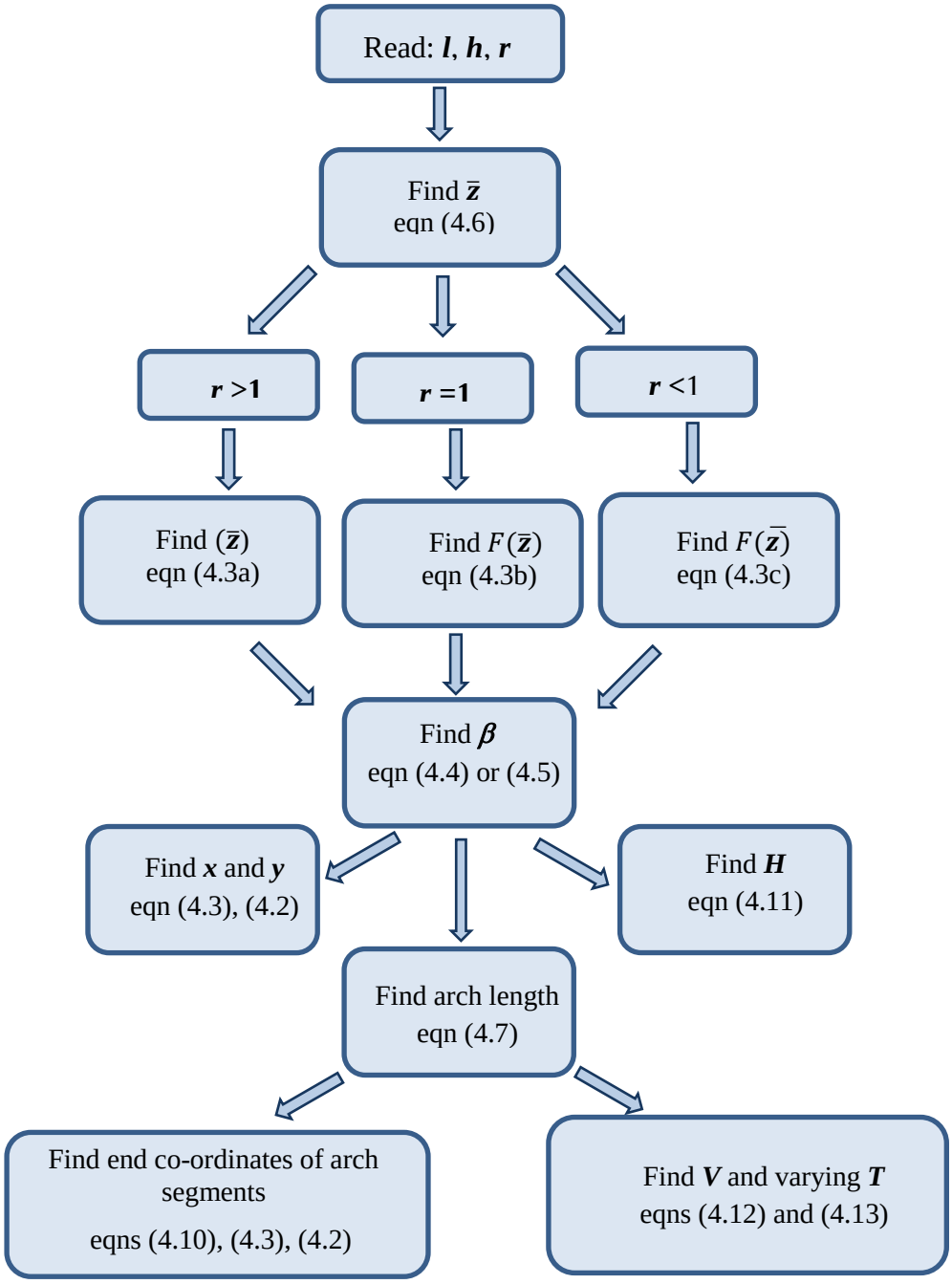

Figure 4. Overall solution procedure.

5. Case study 1: Medium-span arch, r = 2

5.1 Arch geometry

A moment-less arch of span l = 50 m is subjected to permanent load comprising the deck weight, w = 50 kN/m, and arch self weight, q = 25 kN/m, giving the load ratio, $r = w/q = 2$. The cross-section of the arch is 1.47 m x 0.68 m, giving a cross-section area of ~1 m^2. The centre-line profile of the moment-less arch shown in Fig. 5 is calculated according to the process shown in Fig. 4, using Excel. It is found that, for $\rho = 2$, the values of the key parameters are $\bar{z} = 2.364947$ and $\beta = 0.02459838$, and for $\rho = 4$, $\bar{z} = 1.431088$ and $\beta = 0.01300461$. (The precision of the results quoted ensured that the centre-line profile closed very accurately, giving: $y = 0$ at $x = l/2$).

With, r, β, and $h = l/\rho$ known, detailed co-ordinates of the arch profile are found from eqns (4.2) and (4.3), as values corresponding to the parameter, z, selected between its limits of 1 and $\bar{z}$.

The case of $\rho = 2$ is selected to demonstrate the calculation of arch segment geometries, as outlined in Fig. 3. From eqn (4.7), the total length of the arch is:

$$C = \frac{2}{0.02459838}\sqrt{(2.364947^2 - 1)} - 2 \times 50 = 74.249 \text{ m.}$$

For visualisation purposes, it is sufficient to have the centre-line profile of the arch represented by 44 elements (Fig. 5).

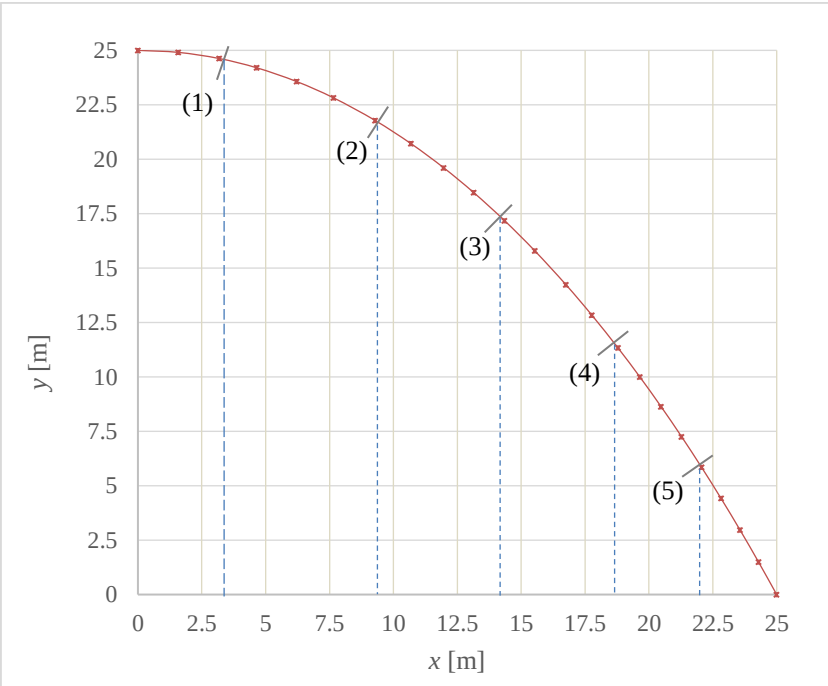

Figure 5. Case study 1. Centre-line profile of a moment-less arch constructed with 11 equal-size segments.

Assuming the arch is to be constructed from 11 equal-size segments, the length of each segment is 6.750 m. In Fig. 5, the ends of segments (1-5) are referenced sequentially, starting from the origin, but they could also start being referenced from the supporting end of the arch. As stated in Section 4.3, in order to start the iterative procedure given by eqn (4.9), the initial value for x_1 can be taken from the co-ordinates used to create the graph; in this case, x_1= 3.1783m.

The iterative process reported here was carried out using Excel. The results, accurate to within 0.4 mm difference between successive values of x^{i+1}_n and x^i_n, are given in Table 1. Values of the *y* co-ordinates (not stated in Table 1) can be found from eqn (4.2) using the corresponding values for *z*.

Table 1. Case study 1. Medium-span arch. Results of the iterative computation for segmental end co-ordinates.

Element end *n*	C_n [m]	*z*	x_n [m]
1	3.375	1.030135	3.340
2	10.125	1.227209	9.397
3	16.875	1.502967	14.369
4	23.625	1.794523	18.475
5	30.375	2.083324	21.962

5.2 Moment-less and conventional arch forms under permanent load

The study presented here concerns the geometry/centre-line profiles of the moment-less, parabolic, and circular arches of the same cross-section, span, and rise. All arches carry the same deck weight. The arch profiles are discretised using line elements in preference to computationally more expensive curved elements, which, in any case, would not match the required geometry of the moment-less arch. In stress and displacement analyses, the number of elements used is such as to ensure smooth stress variations along the arches, and negligible differences between the theoretical and discretised lengths of their centre line profiles (Tables 2-4, Section 5.4).

The results, shown in Figs. 6 (a) and 6 (b) indicate that the profile of the circular arch is distinctly different from the moment-less and parabolic arch configurations. Although circular arches have been predominantly used in in-filled construction, their inclusion in the current analysis is intended to emphasise the effect of structural form on its stress response to loading.

Detailed comparisons of the calculated arch profiles show that, for $\rho = 2$, the maximum difference in the *y* co-ordinates between the moment-less and circular arch configurations

approaches 6 m, for x ranging between 20 and 21 m. For $\rho = 4$, the arch profiles start to converge, with the moment-less and parabolic configurations showing a maximum difference of only 75mm, for x between 17 and 19 m. Despite this, the volume of material in the parabolic arch required to carry the same deck weight, while matching the maximum stress in the moment-less arch, was found to be significantly higher, as discussed in the next section.

(a)

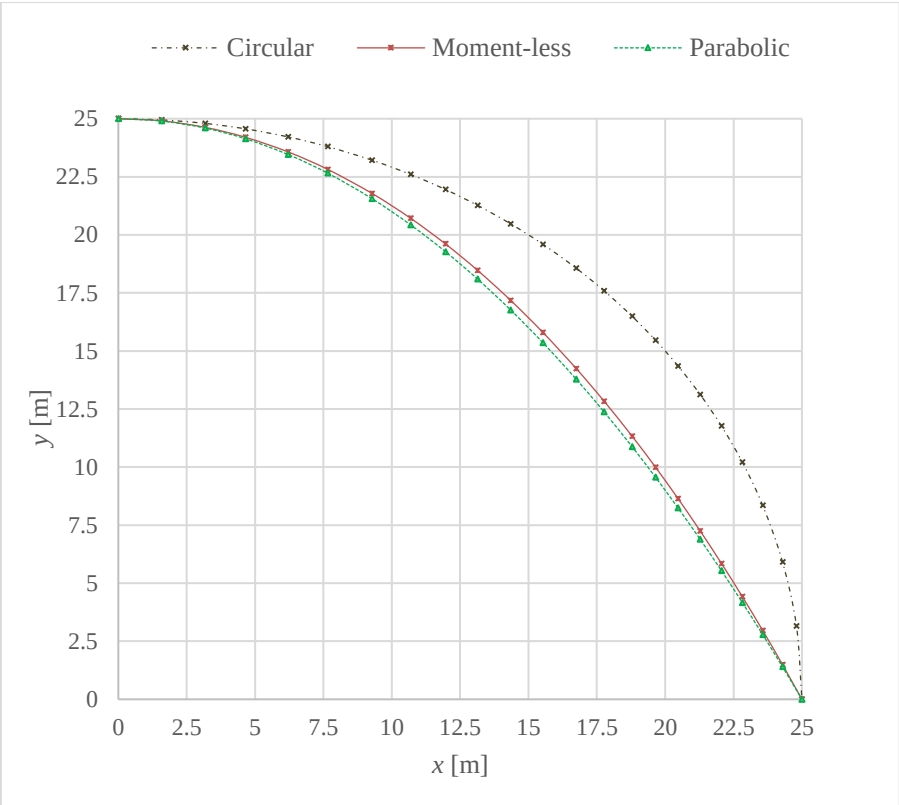

(b)

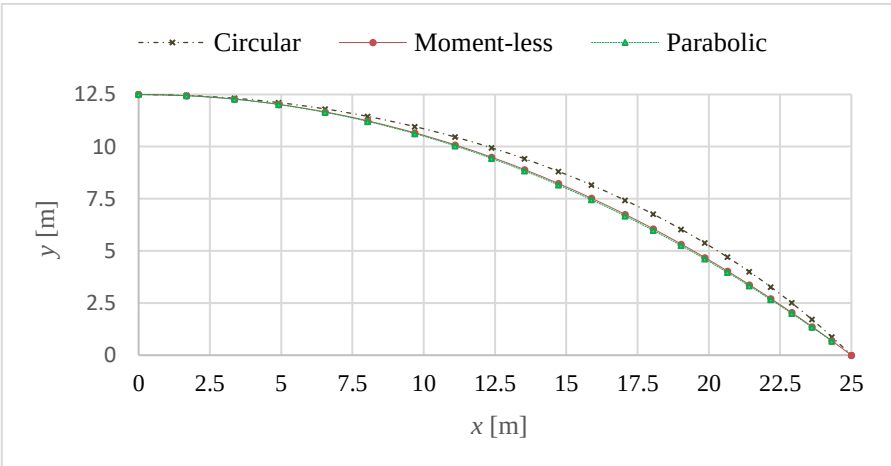

Figure 6. Case study 1. Centre-line profiles of medium-span arches (a) $\rho = 2$, (b) $\rho = 4$.

5.3 Comparisons of material volume

Each of the three arches develops a different level of stress when carrying the same deck weight (uniformly distributed per 1m span). For meaningful comparisons, the same value of the combined (axial + bending) stress is used here - a value corresponding to the maximum compressive stress developing in the moment-less arch. In the case of $\rho = 2$, this target stress value is 2.4MPa, and in the case of $\rho = 4$, it is 2.75 MPa. In order to meet these stresses, the cross section areas of parabolic and circular arches were systematically scaled up, by increasing their section depths by factors 1, 1.5, 2, and 3. As the stresses do not scale directly with the increases in the cross-section area, it was necessary to carry out stress analysis for each scaling factor. This was achieved using ABAQUS software, with the results checked independently by GSA for the case where the depth factor was 1. Both programs use two node beam elements and linear elastic analysis within the small displacement theory. The results showed excellent agreement, with the maximum combined stresses differing by ~0.5%.

The process of finding the correct scaling factor for the depth of the parabolic arch is illustrated in Fig. 7. It can be seen that the factors required to achieve the target stresses matching those of the moment-less arch are ~ 2.2 for $\rho = 2$, and ~1.4 for $\rho = 4$.

A similar analysis carried out for the circular arch showed that the chosen target stress was not achievable. Therefore, its value was increased to match the maximum combined stresses in the parabolic arch, giving: 4.56 MPa for $\rho = 2$, and 3.38 MPa for $\rho = 4$.

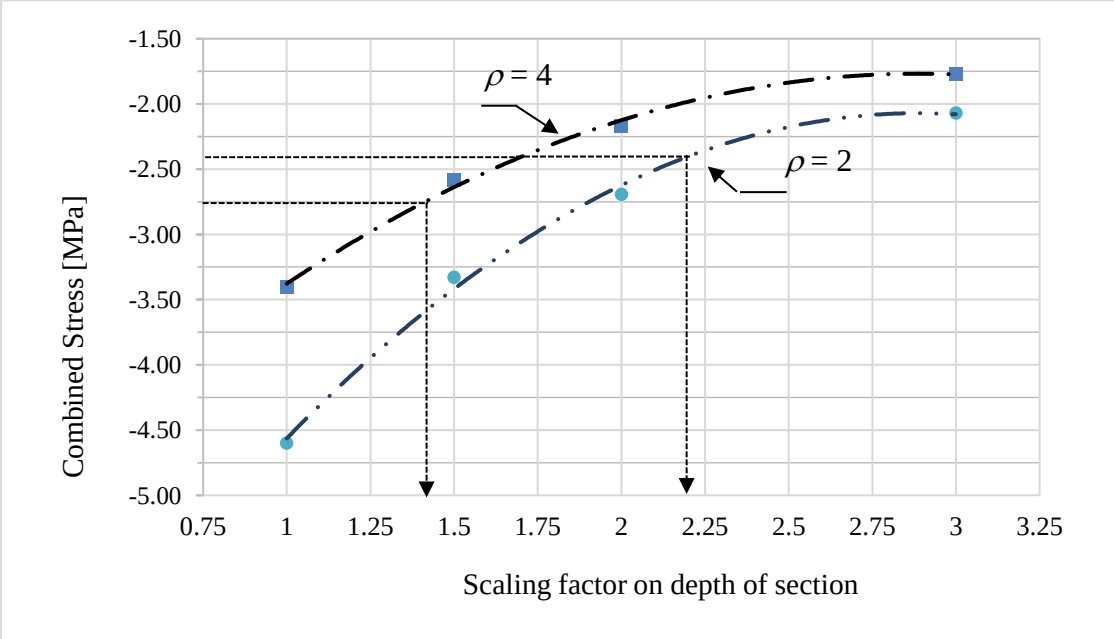

Figure 7. Parabolic arch: scaling factors on depth of section vs combined stress.

The estimated volumes of the material required by the three types of arches were calculated as a product of their arch lengths and cross-section area; the results are summarised in Fig. 8. They show that the circular arch uses a disproportional amount of material when carrying the same deck load, compared to the other two arch forms.

As noted in Section 5.2, the maximum difference between the moment-less and parabolic arch profiles, for $\rho = 4$, was just 75 mm, yet, this still translated to an increase in volume of the parabolic arch by ~50% compared to the moment-less form.

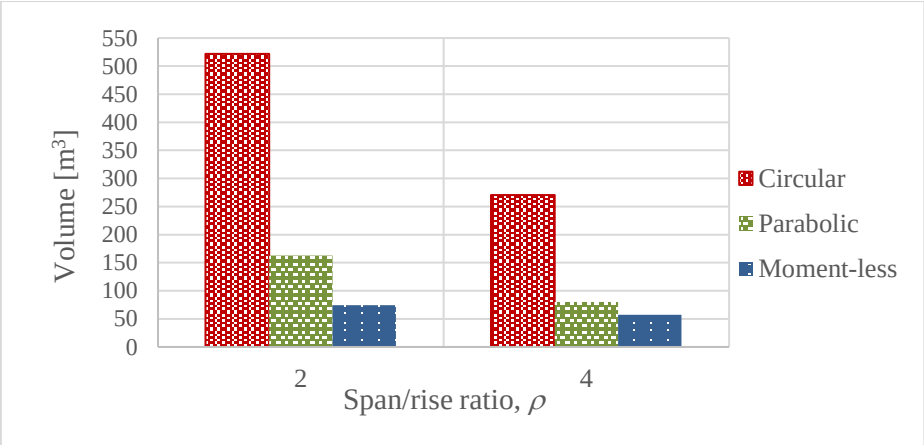

Figure 8. Case study 1. Volumes of material in arches carrying the same deck load, with comparable levels of maximum combined stress.

Figure 9 provides a visual summary of the geometries of the three types of arches using CAD models.

(a)

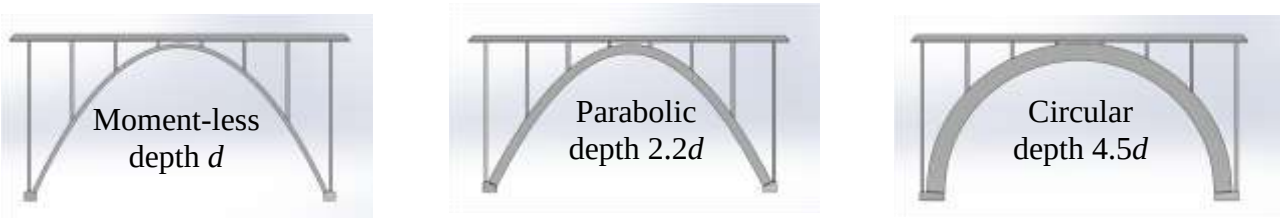

(b)

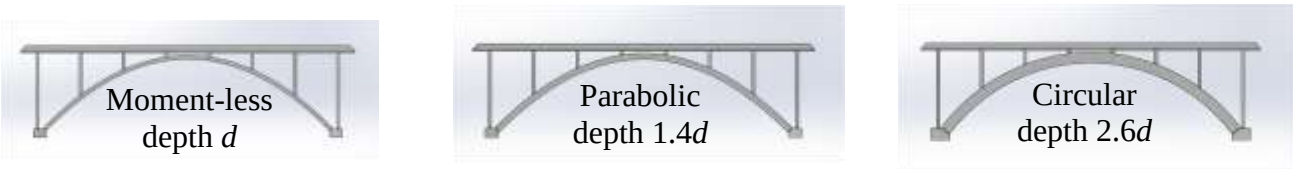

Figure 9. Case study 1. Medium-span arches carrying the same deck weight, (a) ρ =2, and (b) ρ =4. Increases in the cross-section area of the arches were made to ensure the arches reach comparable stresses. CAD modelling: M. Millson, University of Warwick.

5.4 Stress and displacement analyses

5.4.1 Permanent load: inextensible vs elastic model

Results presented in Section 5.3 show that the circular arch does not compete with the moment-less or parabolic form. Therefore, in the remainder of this case study, the focus is placed on the comparison between the parabolic and moment-less forms.

The model of the moment-less arch defined by analytical form-finding presented in [1] is based on the assumption of inextensible behaviour. The permanent load case considered here provides an opportunity for comparing the results from this model with an elastic model offered by the finite element analysis using GSA software (with the results verified by ABAQUS). In the elastic model, the Young's modulus is assumed to be 28 GPa and shear modulus 1.17 GPa. The arch is discretised using 176 elements, giving the discretised arch length of 74.248 m, as opposed to the exact length of the continuous arch of 74.249 m (eqn (4.7)).

(i) High-rise arches ($\rho = 2$)

Results of the stress and displacement analyses for the high-rise arches are shown in Fig. 10, with more detail provided in Table 2. The negative sign indicates compression in relation to stress, and downward movement, in relation to displacement. Results are given at certain characteristic points in the arch, where the combined and axial stresses, and displacements, reach extreme values. The locations of them are different for each arch.

(a)

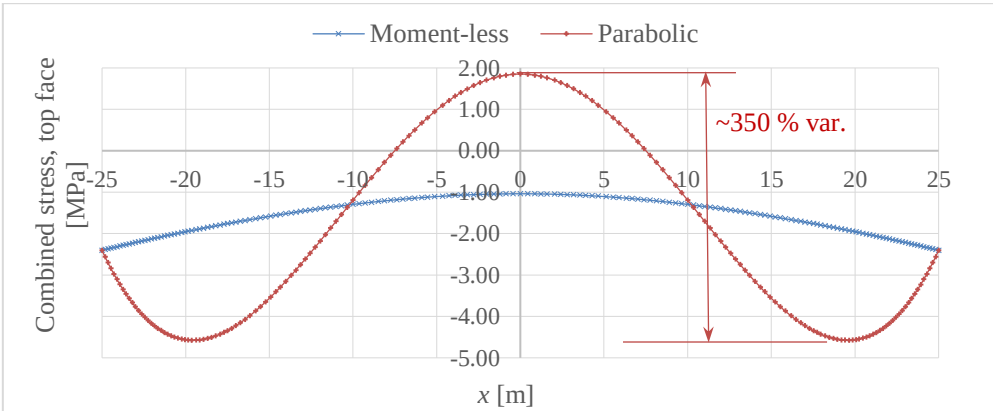

(b)

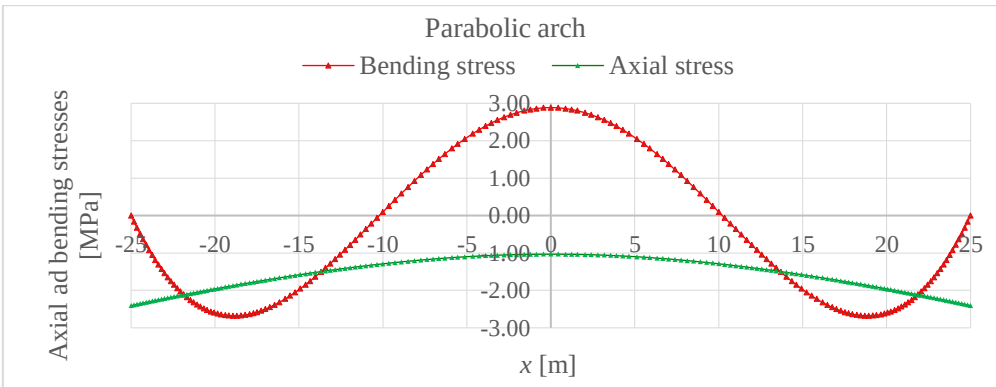

Figure 10. Case study 1. (a) Combined stresses in medium span, moment-less and parabolic arches, (b) Variations in axial and bending stresses in the parabolic arch. (Permanent load, ρ =2).

It can be seen that, due to the elastic effects, the moment-less arch develops a small amount of bending, producing a maximum bending stress of just 2.2% of the axial stress (Table 2). Consequently, the combined axial and bending stresses, and pure axial stresses are practically the same, and the arch works in pure compression. In the case of the parabolic arch, axial stresses are almost identical to those present in the moment-less arch, but bending action dominates the structure's behaviour; the arch develops a tension region and the maximum variation in the combined stress along the arch of almost 350% (Fig. 10). The maximum variation of the combined stress in the arch cross-section is almost two orders of magnitude higher than in the moment-less arch (Table 2).

Table 2. Case study 1. Results for medium-span, moment-less and parabolic arches (Permanent load, $\rho = 2$)

	Moment-less	Parabolic
Axial stress [MPa]	**-2.40 MPa** (x = ±25 m) -1.92 MPa (x =±19.644 m) -1.86 MPa (x =±18.936 m) -1.01 MPa (x = 0 m)	**-2.41** MPa (x = ± 25 m) -1.93 MPa (x =±19.644 m) -1.88 MPa (x =±18.936 m) -1.03 MPa (x = 0 m)
Combined stress (top face)	**-1.93 MPa** (x =±19.644 m) -1.87 MPa (x =±18.936 m) -1.04 MPa (x = 0 m)	**-4.58 MPa** (x =±19.644 m) -4.55 MPa (x =±18.936 m) +1.85 MPa (x = 0 m)
Bending stress	-0.01MPa (x =±19.644 m) -0.01MPa (x =±18.936 m) ±**0.02 MPa** (x = 0 m)	±2.65 MPa (x =±19.644 m) **±2.68 MPa** (x =±18.936 m) ±2.88 MPa (x = 0 m)
Maximum variation of combined stress in the cross-section	**-0.99 ÷ -1.04 MPa** (x = 0 m) (difference: 0.05 MPa)	**-0.01 ÷ - 4.23 MPa** (x = ± 21.867m) (difference: 4.22 MPa)
Vertical displacement	-1.4 mm (x =±17.949 m) -**2.6** mm (x = 0 m)	**-11.9** mm (x =±17.949 m) +11.7 mm (x = 0 m)
Resultant displacement	-1.4 mm (x =±18.217 m) -**2.6 m**m (x = 0 m)	**-22.8 mm** (x =±18.217 m) +11.7 mm (x = 0 m)
Vertical reaction	2178 kN	2174 kN
Horizontal reaction	1016kN	1032 kN
Arch length (exact)	74.249 m	73.947 m
Arch length (176 elements)	74.248 m	73.946 m

Note: Maximum values shown in bold

It is found that the axial forces, horizontal and vertical reactions obtained from the inextensible model are in excellent agreement with those predicted by the elastic, finite element model. The results indicate that the elastic effect, measured by the level of bending is negligible. The length of the parabolic arch of 73.947 m is 0.302 m shorter than the length of the moment-less structure and, therefore, the vertical reaction is proportionally lower (Table 2). The horizontal reaction is higher, because of the higher level of bending.

Figure 11 shows the profile of vertical displacements for the two arches; it can be seen that it mirrors the pattern of the combined stresses developing in them, with the parabolic arch experiencing both downward and upward displacements of a magnitude several times higher than that observed in the moment-less form (Table 2).

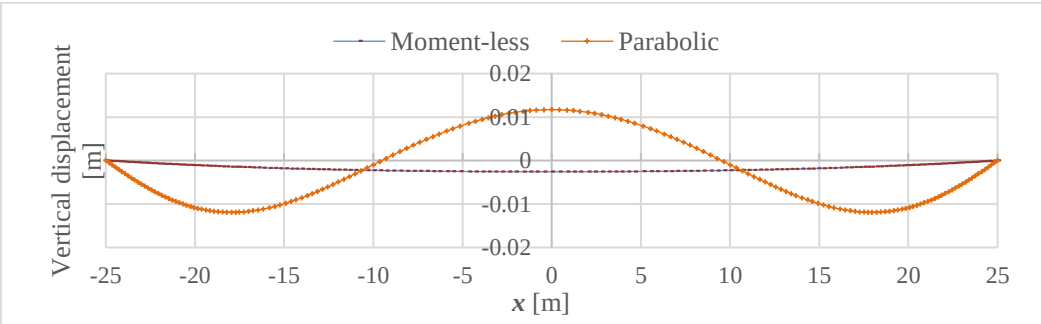

Figure 11. Case study 1. Variations in vertical displacements in medium-span, moment-less and parabolic arches. (Permanent load, ρ =2).

Overall, the results indicate that the high-rise moment-less arch develops a much lower level of stress and deflection than the parabolic form, and its elastic straining under permanent load is insignificant.

(ii) Low-rise arches (ρ = 4)

The arch is discretised using 88 elements, giving the discretised arch length of 57.439 m, with the exact length of a continuous rigid arch of 57.440 m. Results for this case are summarised in Table 3. Again, it is found that the axial forces, together with horizontal and vertical reactions obtained from analytical form-finding/inextensible model are in excellent agreement with those from the elastic, finite element model. They indicate, again, that the elastic effect is insignificant.

The length of the parabolic arch of 57.390 m is 0.050 m shorter than for the moment-less arch and, therefore, its vertical reaction (Table 3) is proportionally lower. The horizontal reaction is higher, because of the higher level of bending.

It is found that the pattern of stress remains unaltered from the previous case (ρ = 2), except that the parabolic arch no longer develops a tension region. In the moment-less arch, the maximum bending stress is now slightly raised, reaching 3.6% of the axial stress (Table 3). This value is still an order of magnitude smaller than in the parabolic arch, in which the maximum bending stress constitutes 38% of the axial stress, the maximum variation of the

combined stress along the arch length is 278%, and the maximum variation of the combined stress in the cross-section, an order of magnitude higher than in the moment-less form. These results are surprising, bearing in mind that the maximum difference in the centre-line profiles of the two arches, indistinguishable by eye, is just 75 mm (Section 5.2).

The parabolic arch no longer exhibits upward deflections, and its level of displacements is comparable to that of the moment-less arch, although it still follows a distinctly different pattern, as was the case with the high-rise structure shown in Fig. 11.

Table 3. Case study 1. Results for medium-span, moment-less and parabolic arches (Permanent load, $\rho = 4$).

	Moment-less	Parabolic
Axial stress	**-2.75 MPa** (x = ±25 m) -2.48 MPa (x =±20.256 m) -2.42 MPa (x =±18.947 m) -1.92 MPa (x = 0 m)	**-2.76 MPa** (x = ± 25 m) -2.49 MPa (x =±20.256 m) -2.42 MPa (x =±18.947 m) -1.93 MPa (x = 0 m)
Combined stress (top face)	**-2.51 MPa** (x =±20.256 m) -2.45 MPa (x =±18.947 m) -1.99 MPa (x = 0 m)	**-3.37 MPa** (x =±20.256 m) -3.35 MPa (x =±18.947 m) -1.21 MPa (x = 0 m)
Bending stress	±0.02 MPa (x =±20.256 m) ±0.03 MPa (x =±18.947 m) ±**0.07 MPa** (x = 0 m)	±0.88 MPa (x =±20.256 m) ±**0.93 MPa** (x =±18.947 m) ±0.72 MPa (x = 0 m)
Maximum variation of combined stress in the cross-section	**-1.85 ÷ -1.99 MPa** (x = 0 m) (difference: 0.14 MPa)	**-1.50 ÷ - 3.35 MPa** (x = ± 18.947m) (difference: 1.85 MPa)
Vertical displacement	-2.3 mm (x =±15.881 m) **-4.1 mm** (x = 0 m)	**-4.7 mm** (x =±15.881 m) -0.5 mm (x = 0 m)
Resultant displacement	-2.3 mm (x =±16.505 m) **-4.1 mm** (x = 0 m)	**-5.4** mm (x =±16.505 m) -0.5 mm (x = 0 m)
Vertical reaction	1968 kN	1967 kN
Horizontal reaction	1922 kN	1929 kN
Arch length (exact)	57.440 m	57.390 m
Arch length (discretised, 88 elements)	57.439 m	57.389 m

Note: maximum values shown in bold

The small amount of bending and displacement, combined with unchanged axial stresses in the moment-less arch indicate that the inextensible model of the structure, defined through analytical form-finding, approximates the elastic model very closely. This conclusion applies to both high and medium-rise arches, with $\rho = 2$, and 4, respectively.

5.4.2 Variable load

Having established advantages of the moment-less arch over the conventional parabolic form in terms of its response to permanent load, it is interesting to examine the behaviour of the two arches under variable load comprising permanent + live (transient) loads. In this case, the input data is the same as that given in Section 3.1, but the arches are additionally subjected to a patch load of 25 kN/m, constituting 50% of the deck weight and acting on the left half-span.

(i) High-rise arches ($\rho = 2$)

Figure 12 presents results for the combined stresses developing in the high-rise arches. It can be seen that they follow a similar pattern in the tension region. Detailed numerical results in this case show a maximum value of +7.11 MPa at x = +12.564 m for the moment-less arch, and +7.06 MPa at x = +8.124 m for the parabolic one. The tension region in the moment-less arch extends for a slightly longer distance, compared to the parabolic arch. While the maximum tensile stress is approximately the same for both arches, the maximum combined compressive stress is ~20% higher in the parabolic arch: -12.17 MPa at x = -15.832, as opposed to -10.13 MPa at x = -12.564 m in the moment-less one. The maximum combined stress variation in the cross-section of the parabolic arch is also found to be ~ 20% higher.

The displacement profile of each arch is found to be very similar, mirroring the pattern adopted by the combined stress shown in Fig. 12. Detailed results reveal that, in the case of the moment-less arch, the maximum vertical downward displacement is -86.03 mm at x = -12.855 m, and the upward one: +82.75 mm at x = +13.423 m. The resultant displacements are approximately twice these values. The maximum downward displacement for the parabolic arch is larger: -93.57 mm at x =-14.349 m, but the upward displacement somewhat lower: +78.92 mm at x = +11.657 m. The resultant displacements, are again, approximately twice these values.

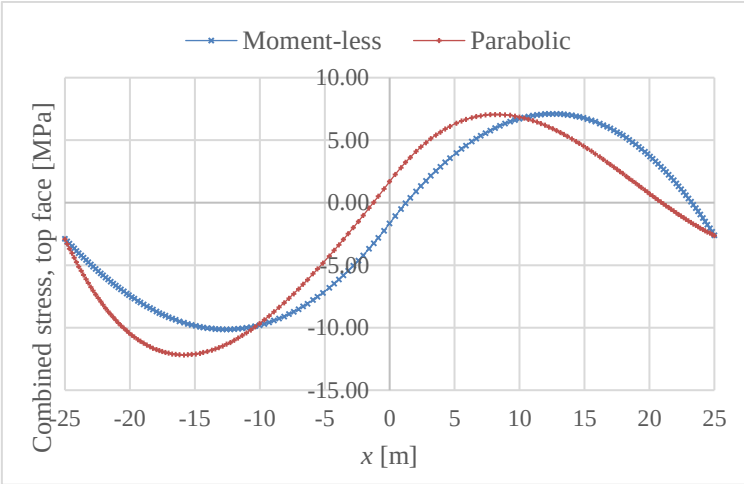

Figure 12. Case study 1. Combined stresses in medium-span, moment-less and parabolic arches. (Variable load, ρ =2)

Apart from a comparable performance of the two arches with regard to the maximum tensile stresses, it is also found that the moment-less arch develops a lower value of maximum combined compressive stress, lower maximum variation of the combined stress in the cross-section, and lower downward displacement.

(ii) Low-rise arches (ρ = 4)

It is found in this case that the behaviour of the moment-less and parabolic arches is comparable, in terms of the combined stresses developing in the tension region (top face), with the maximum values of + 6.13 MPa at x = +12.377 m for the moment-less arch, and +5.81 MPa at x = +11.06 m for the parabolic one. The maximum combined compressive stresses (top face) are also similar: -11.69 MPa at x = -14.090 m for the parabolic arch, and -11.11 MPa at x = -12.377 m for the moment-less one. The maximum combined stress ranges in the cross-section of the arches are similar: -11.11 MPa ÷ +6.13 MPa at x = ±12.377 m, for the moment-less arch, compared to -11.69 MPa ÷ +6.53 MPa at x = -14.090 m in the parabolic form.

6. Case study 2: Large-span moment-less arch, *r* = 0.714

A large-span moment-less arch analysed here resembles the iconic Hoover Dam Bridge, shown in Fig. 13. The aim of the design of this structure was to bring its bending moments under permanent load to zero, i.e., achieve a funicular form.

The moment-less arch form simulating that of the Hoover Dam Bridge has a span l = 323 m and rise h = 87.297 m, giving the span/rise ratio, ρ = 3.7. The structure is composed of two reinforced concrete arches of rectangular hollow section, with outer dimensions: 6.096 m by 4.267 m, and inner dimensions: 5.385 m by 3.353 m. Each arch is subjected to a permanent load comprising the deck weight, w = 145.935 kN/m, and arch weight, q = 204.3 kN/m, giving the deck weight/arch weight ratio, r = 0.714. This ratio indicates that the deck weight

is light compared to the arch weight, but the main concerns in the design of the Hoover Dam Bridge was creep due to high temperatures experienced on site. The arch is made of high-strength concrete having a characteristic strength of 70 MPa. Thus, the Young's modulus used in the finite element analyses was 35 GPa, as opposed to 28 GPa in Case study 1.

Figure 13. Hoover Dam Bridge, 2011.
https://unsplash.com/s/photos/hoover-dam
(Public domain image)

The centre-line profile of the moment-less arch shown in Fig. 14 is calculated according to the process shown in Fig. 4. It produced the following values for the key parameters: $\bar{z}$ =1.510748659 and β = 0.003717509, from which the required *x* and *y* co-ordinates were obtained. The structure was represented by 108 beam elements, giving the discretised arch length of 378.607 m, as opposed to the exact length of 378.611 m.

6.1 Comparison of arch profiles

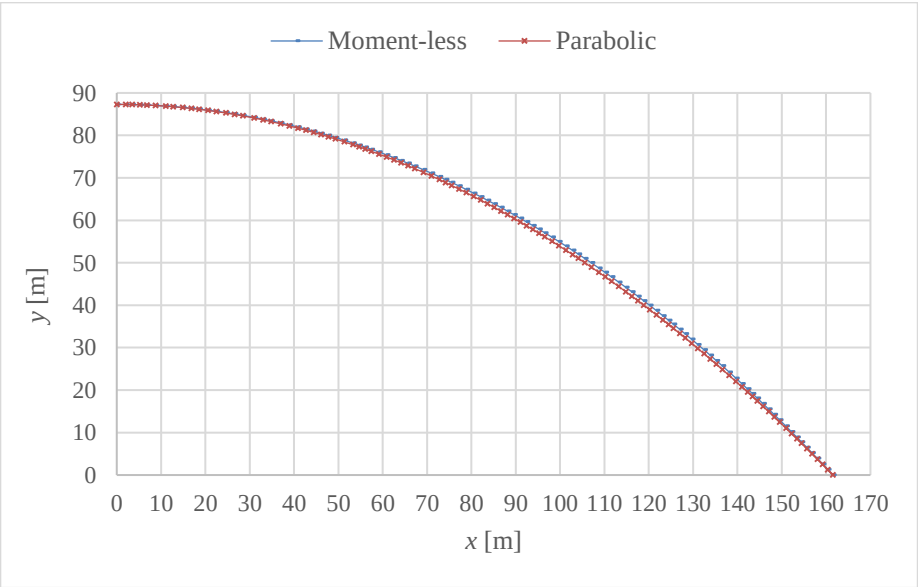

Figure 14. Case study 2. Centre-line profiles of large-span, moment-less and parabolic arch forms.

Detailed results indicated that the maximum difference in the *y* co-ordinates of the moment-less and parabolic arches was just over 1m, for *x* between ±102.799 m and ±120.162 m. Such a difference is hardly noticeable by eye, but, as shown in the subsequent analyses, it makes a significant difference to the stress response of the two arches.

6.2 Stress and displacement analyses

6.2.1 Permanent load

The moment-less and parabolic arches are subjected to the same deck and arch weight as that stated in the opening paragraphs of Section 6. The results are summarised in Table 4.

Table 4. Case study 2. Results for large-span, moment-less and parabolic arches (Permanent load, $\rho = 0.714$).

	Moment-less	Parabolic
Axial stress	**-10.43 MPa** (x = ±161.499 m) -9.15 MPa (x =±128.210 m) -8.88 MPa (x= ±120.162 m) -6.90 MPa (x = 0 m)	**-10.46 MPa** (x = ± 161.499m) -9.20 MPa (x =±128.210 m) -8.93 MPa (x= ±120.162 m) -6.96 MPa (x = 0 m)
Combined stress (top face)	**-9.26 MPa** (x =±128.10 m) -7.20 MPa (x = 0 m)	**-12.98 MPa** (x =±128.210 m) -3.90 MPa (x = 0 m)
Bending stress	±0.14 MPa (x =±120.162 m) ±**0.30 MPa** (x = 0 m)	±**3.88 MPa** (x =±120.162 m) ±3.06 MPa (x = 0 m)
Maximum variation of combined stress in the cross-section	**-6.60 ÷ -7.20 MPa** (x = 0 m) (difference: 0.6 MPa)	**-5.05 ÷ - 12.81 MPa** (x = ± 120.62m) (difference: 7.76 MPa)
Vertical displacement	-42.49 mm (x =±105.304 m) **-74.45** mm (x = 0 m)	**-97.56 mm** (x =±105.304 m) -8.03 mm (x = 0 m)
Resultant displacement	-41.9 mm (x =±108.719 m) **-74.5 mm** (x = 0 m)	**-118.2 mm** (x =±108.719 m) -8.0 mm (x = 0 m)
Vertical reaction	62 240 kN	62 170 kN
Horizontal reaction	54 930 kN	55 390 kN
Arch length (exact)	378.611 m	377.895 m
Arch length (discretised, 108 elements)	378.607 m	377.889 m

Note: Maximum values shown in bold

It is found that the values of the reactions and axial forces are the same for the inextensible and elastic models of the moment-less arch. It can be seen that the combined stresses in the moment-less arch vary in a gentle manner, as do the displacements (Table 4). A small amount of bending is noted, constituting 4.2% of the axial stress. By contrast, the maximum bending stress in the parabolic arch constitutes 43% of the axial stress, and the arch experiences 333% variation in the combined stress along its length. Similar to Case study 1, $\rho = 4$, the maximum combined stress variation in the cross-section of the parabolic arch is an order of magnitude higher, compared to the moment-less form, despite small differences in the centre-line profiles of the two arches. Furthermore, the parabolic arch displaces in a non-uniform manner, with the largest resultant displacement at $x = 108.719$ m, and the smallest, in the centre (Table 4). This pattern of displacement follows that of the combined stress along the length of the arch.

6.2.2 Variable load

In addition to the permanent load, here the arches are subjected to a patch load of 72.968 kN/m (50% of the deck weight), acting on the right hand half-span. Figure 15 shows the pattern of combined stresses in the two arches. Their behaviour is found to be comparable when considering the maximum combined stress (top face) in the tension region, but the parabolic arch exhibits ~ 20% higher level of the maximum compressive stress and 24% higher combined stress variation in the cross section.

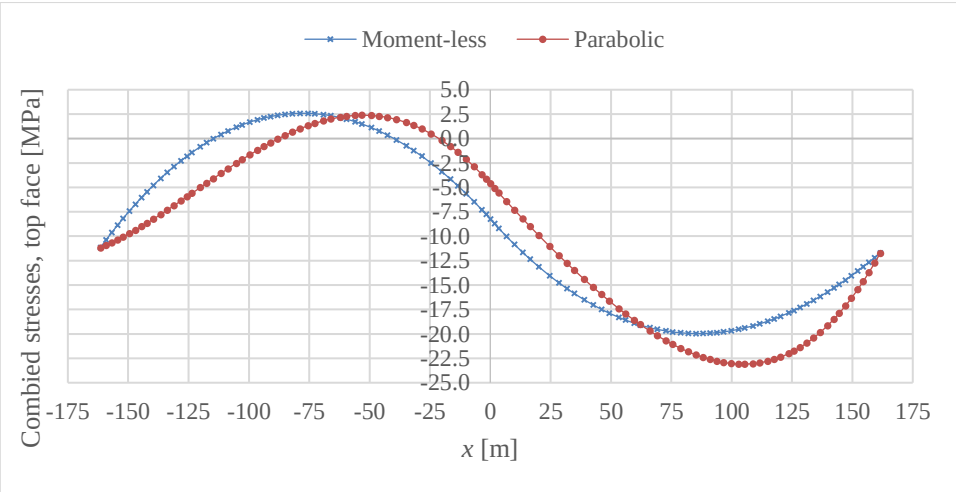

Figure 15. Case study 2. Combined stresses in large-span, moment-less and parabolic arches. (Variable load, $\rho = 0.714$).

6.2.3 Permanent load. Discrete load transfer

It is interesting to examine the effect of discrete load transfer from the deck to the arch via the spandrel columns, shown in Fig. 13. There are ten columns in total, with the outer columns

coming to rest at the end supports of the arch. The columns are assumed to be pin-jointed and placed at a constant spacing of 35.889 m along the arch span. The deck is analysed by GSA as a multi-span beam resting on columns. The resulting reactions at the deck supports (points corresponding to the locations of the columns), are transferred down to the arch. The values of the loads (quoted from left to right) were found to be: 2087 kN, 5884 kN, 5097 kN, 5268 kN, 5232 kN, with the values mirrored for the other half of the span. The load discretisation does not correspond exactly to that shown in Fig. 13, because we are considering the deck loading confined just to the span of the arch, not beyond. The results of the analysis are given in Table 5.

Table 5. Large-span moment-less and parabolic arches subjected to point loads applied by open spandrel columns (Permanent load, $\rho = 0.714$).

	Moment-less	Parabolic
Axial stress	**-10.23 MPa** (x = ±161.499 m) -8.84 MPa (x =±125.610 m) -6.90 MPa (x = 0 m)	**-10.26 MPa** (x = ± 161.499m) -8.89 MPa (x =±125.610 m) -6.96 MPa (x = 0 m)
Combined stress (top face)	**-10.77 MPa** (x =±125.610 m) -6.48 MPa (x = 0 m)	**-14.54 MPa** (x =±125.610 m) -3.17 MPa (x = 0 m)
Bending stress	±**1.93 MPa** (x =±125.610 m) ±0.43 MPa (x = 0 m)	±**5.65 MPa** (x =±125.610 m) ±3.17 MPa (x = 0 m)
Maximum variation of combined stress in the cross-section	**-6.91 ÷ -10.77 MPa** (x =±125.610m) (difference: 3.86 MPa)	**-3.23 ÷ - 14.54 MPa** (x = ± 125.610m) (difference: 11.31MPa)
Vertical displacement	**-75.7 mm** (x =±17.943 m) -75.1 mm (x = 0 m)	**-97.1 mm** (x =±105.304 m) +7.6 mm (x = 0 m)
Resultant displacement	**-75.8 mm** (x =±17.943 m) -75.1 mm (x = 0 m)	**-117.3 mm** (x =±108.719 m) +7.6 mm (x = 0 m)
Vertical reaction	62 240 kN	62 170 kN
Horizontal reaction	54 930 kN	55 390 kN

Note: Maximum values shown in bold

Comparisons of the results presented in Table 5 with those for the case of the uniform deck load being transferred to the arch (Table 4) show that the reactions in each case remain unchanged, and there is no significant change in maximum displacements of the two arches, although their locations have moved somewhat. The maximum value of the combined stress in the moment-less arch has gone up from 9.26 MPa to 10.77 MPa, a 10.9% increase, and in the parabolic arch, from 12.98 MPa to 14.54 MPa, a 12.0% increase. The maximum variation in the combined stress across the cross-section is now 3.86MPa for the moment-less arch, and

11.31 MPa for the parabolic one. The maximum bending stress in the parabolic arch now constitutes 64% of the axial stress, compared to 22% for the moment-less arch.

7. Discussion

The case of permanent load used in the two case studies provides the main focus of this research, to show that the moment-less arch resists this load much more efficiently than the conventional, parabolic form. Consequently, it requires less material. It is assumed here that the permanent load is statistically prevalent; if it is not, then the load that fits this description should be used in shaping the moment-less arch. Since it is not possible to come up with one optimised arch profile to suit all load cases, it is logical to use statistically prevalent load to define the arch configuration. This will produce the lowest stress state for the majority of the time, which enhances a structure's durability. It is, of course, necessary to check the structure for all ultimate load combinations. If, at this stage, the stresses exceed the design strength of material, it is necessary to change the cross-section area of the arch and re-calculate its profile, as the ratio of deck weight/arch weight would change. This, however, constitutes a usual iterative design process.

The assumption of an inextensible behaviour, on which the analytical model of the moment-less arch is built, has been tested against the elastic finite element model offered by the GSA software, the results of which were successfully verified by ABAQUS. A maximum difference of 1% was recorded in the case of very small bending stresses appearing in the moment-less arch when discussing Case study 1, permanent load, span/rise of 2. The small amount of bending in the moment-less arch, observed in all load cases, justifies the use of term 'funicular' or 'moment-less', provided it is understood that a small amount of bending will develop in a real structure.

Case study 2, related to the Hoover Dam Bridge, includes the analysis of the effect of a discrete load transfer from the deck to the arch via the columns. The results indicate that the moment-less arch model performs well in this case, with the change having a more adverse effect on the parabolic arch. In reality, the point loads would be uniformly distributed along the width of each column. This would reduce the increases in the observed stresses, but not alter the conclusions reached with regard to the performance of the two forms of arches.

It is possible to generate a moment-less arch form computationally by applying upward forces to a discretised model using bar, or cable,elements of zero bending stiffness. Such a computational form-finding module is available in GSA software, and has been used to compare the results from analytical form finding of the moment-less arch. Provided a sufficient number of elements is used, excellent agreement was achieved between the discrete shape prediction by GSA, and that of analytical form-finding. It is important to note that, while an assumed inelastic model deforms further under permanent load when elasticity is added to the structure, so does the computationally found funicular shape of an elastic (extensible) structure. The additional deformation of the inextensible model is intuitively obvious, but it is less so in the case of computationally found elastic model. An explanation can be provided using a simple example of a straight-line chain hanging under its own weight.

When the shape of the chain is ‘frozen’ the structure acts as a column subjected to its own weight. The stress reversal is accompanied by a further deformation of the column, because unstrained lengths of the chain and the column are different. In conclusion, the inverted hanging chain model can produce a precise stress reversal without deformation only in the case of an inextensible chain.

Computational form-finding methods are useful and readily available numerical tools, but their accuracy depends on the level of discretisation. A fine mesh requires a greater computational effort to generate discretised funicular forms compared to analytically defined cases. Unlike the analytical solution presented in this paper, a computational approach cannot produce a family of moment-less arches just by changing a few input parameters.

8. Summary and conclusions

The work presented here is a follow-on study of 2-pin moment-less arches of constant cross-section. The arches are shaped by statistically prevalent, permanent load comprising the weight of the deck and the arch, as described in [1]. The results highlight advantages of moment-less forms over conventional structures, mostly of parabolic configuration. Circular arches are included, but not studied in detail; they were used to emphasise the dramatic effect that arch configuration can have on a structure’s response to loading and volume of material required to resist it.

In order to bring the moment-less arch model closer to practical application, this paper offers guidance, in the form of flow charts explaining the use of analytical form-finding in shaping moment-less arches. The solution for their centre-line profiles depends on two key parameters: $\bar{z}$ and β. As these depend only on basic input variables, it is possible to generate a database of their values, to cover a majority of practical cases.

There are numerous advantages of the proposed analytical approach over computational form-finding. They lie in (i) a reduced computational effort required to find the centre-line profile of the arch, (ii) providing solutions for horizontal and vertical reactions, the varying axial force, and (iii) defining the total arch length and segmental arch end co-ordinates to facilitate the design of a prefabricated construction. The derivation of the equation describing the length of the moment-less arch is general; it covers any ratio of deck weight/arch weight that influences the arch profile.

Comparative studies of the moment-less and parabolic arches included a test of the assumption of inextensible behaviour of the analytical moment-less arch. This test was carried out using finite element analyses of an elastic structure, and commercial software. The test was applied to medium and long-span arches of different span/rise, and deck weight/arch weight ratios. The results confirm that the elastic effects resulting in additional bending stresses and displacements in the moment-less arch are insignificant for the case of the permanent load used to shape the arch.

It is generally accepted that the structure must withstand ultimate loads comprising permanent and variable loads, with the appropriate factors of safety. However, it is suggested here that permanent load, assumed to be statistically prevalent, should be used in shaping the moment-less arch profile, to improve its lifespan.

It is shown here that, in the case of permanent load, the maximum level of stress and displacement in the high-rise parabolic arch is an order of magnitude higher than in the moment-less form, with the maximum combined stress variation in the cross-section of the arch almost two orders of magnitude higher. In the case of low-rise arches, the profile of the parabolic arch closely resembles that of the moment-less form. However, the structure still exhibits a higher level of maximum stress and displacement, with the maximum combined stress variation in the cross-section of the arch an order of magnitude higher. The sensitive relationship between stress and form calls for high precision in construction to ensure that the advantages offered by the moment-less arch are kept. This challenge can be met through pre-fabricated construction and employment of modern, precise measurement, manufacturing techniques.

Our study shows that, under variable load involving permanent and live loads, which cause significant elastic effects in both types of arches, the levels of stress and displacement in moment-less and parabolic arches are comparable. However, the maximum stress variation in the arch cross-section is still higher in the parabolic arch. Overall, a high level of variation of the combined stress variation in the cross-section of the parabolic arch is observed. The above conclusions have been reached after the analysis of twelve arch structures grouped into two case studies, with additional two examples of circular arch forms.

In all cases presented here, a common assumption is used that the uniformly distributed deck load is transferred directly to the arch. This assumption holds when the deck is suspended from the arch by closely spaced hangers, but may require attention when the deck weight is transferred to the arch via less frequently spaced columns, as in the case of the Hoover Dam Bridge. A brief study of the effect of this type of load transfer has been included here and the results confirm that the proposed model of the moment-less arch works well in this case; the structure experiences relatively small increases in bending stresses, compared to the parabolic arch. In practice, balance needs to be struck between theoretical accuracy, improved by the presence of additional columns, aesthetics, and cost.

It is suggested here that the idea behind the conventional design approach of minimising the amount of material in a structure, regardless of its overall configuration, is misplaced. A different configuration, such as the one offered by the moment-less arch form, brings not only material savings, but also enhanced durability through the reduction of stress levels and stress variations. These characteristics, observed in highly optimised objects found in nature, are very important from a durability perspective – a key concern for our future infrastructure.

Appendix A. Arch length

With reference to Fig. 1, the length of the moment-less arch, *C*, is given by:

$$C = 2\int_{0}^{l/2} \sqrt{1 + y'^2}\,dx. \tag{A1}$$

Noting that $z = \sqrt{1 + y'^2}$ and *x* is known in terms of the parameter *z*, so that

$$dx = \frac{dx}{dz}dz,$$

eqn (A1) can be written as:

$$C = 2\int_{z=1}^{z=\bar{z}} z\,\frac{dx}{dz}dz, \tag{A2}$$

where *x* is given by eqn (2.2).

Selecting the case r >1, for which the relevant equations are (2.2) and (2.2a) gives:

$$x = \frac{1}{\beta}\cosh^{-1}z - \frac{r}{\beta\sqrt{r^2-1}}\ln\left[\frac{\sqrt{r+1}+\sqrt{r-1}}{\sqrt{r+1}-\sqrt{r-1}}\cdot\frac{z+\sqrt{z^2-1}+r-\sqrt{r^2-1}}{z+\sqrt{z^2-1}+r+\sqrt{r^2-1}}\right] \tag{A3}$$

Differentiating eqn (A3) w.r.t. *z*, gives:

$$\begin{aligned}\frac{dx}{dz} &= \frac{1}{\beta\sqrt{z^2-1}} - \frac{r}{\beta\sqrt{z^2-1}}\left[\frac{z+\sqrt{z^2-1}}{\left(z+\sqrt{z^2-1}\right)(z+r)}\right] \\ &= \frac{1}{\beta}\left[\frac{1}{\sqrt{z^2-1}} - \frac{r}{\sqrt{z^2-1}(z+r)}\right]\end{aligned} \tag{A4}$$

and leads to:

$$C = \frac{2}{\beta}\int_{1}^{\bar{z}}\left[\frac{z}{\sqrt{z^2-1}} - \frac{rz}{\sqrt{z^2-1}(z+r)}\right]dz. \tag{A5}$$

The evaluation of the first integral gives:

$$\int_{1}^{\bar{z}} \frac{z}{\sqrt{z^2-1}}dz = \sqrt{\bar{z}^2-1}. \tag{A6}$$

The evaluation of the second integral can be done using a substitution:

$z = \cosh\theta$, $dz = \sinh\theta$, so that:

$$r\int_{1}^{\bar{z}} \frac{z}{\sqrt{z^2-1}\,(z+r)}dz = \int \frac{\cosh\theta\,\sinh\theta\,d\theta}{\sinh\theta(\cosh\theta + r)} =$$

$$= \int \frac{(\cosh\theta + r) - r}{(\cosh\theta + r)}d\theta = \int d\theta - r\int \frac{d\theta}{\frac{1}{2}(e^{\theta} + e^{-\theta}) + r}.$$

Noting that $\theta = \cosh^{-1}z$ and $e^{\theta} = z + \sqrt{z^2-1}$, the above leads to:

$$r\int_{1}^{\bar{z}} \frac{z}{\sqrt{z^2-1}\,(z+r)}dz =$$
$$= r\left[\cosh^{-1}\bar{z} - \frac{r}{\sqrt{r^2-1}}ln\left(\frac{\sqrt{r+1}+\sqrt{r-1}}{\sqrt{r+1}-\sqrt{r-1}}\cdot\frac{\bar{z}+\sqrt{\bar{z}^2-1}+r-\sqrt{r^2-1}}{\bar{z}+\sqrt{\bar{z}^2-1}+r+\sqrt{r^2-1}}\right)\right] \quad \text{(A7)}$$

Therefore, from eqns (A6), (A7), and (A5) we get:

$$C = \frac{2}{\beta}\sqrt{\bar{z}^2-1} - 2r\left[\frac{1}{\beta}\cosh^{-1}\bar{z} + F(\bar{z})\right]. \quad \text{(A8)}$$

When

$$z = \bar{z},\ \ x = \frac{l}{2}\ ,$$

the total length of the arch becomes:

$$C = \frac{2}{\beta}\sqrt{\bar{z}^2-1} - rl, \quad \text{(A9)}$$

quoted as eqn (2.7) in Section 2.2.

Interestingly, the derivative *dx*/*dz* turns out to be the same for all cases of *r* (*r* >1, *r* = 1, *r* < 1), so the integral (A2) leads to the same solution as that given in eqn (A9).

Acknowledgement

This work was supported by the Leverhulme Trust [grant ref: EM-2020-059/9].

References

[1] Lewis, W J. Mathematical model of a moment-less arch. *Proc. Royal Soc. A.* 2016*;* **472**, (doi.org/10.1098/rspa.2016.0019).

[2] Timoshenko, S P. & Young, D H. *Theory of structures*. New York: McGraw-Hill 1961.

[3] Karnovsky, I A. *Theory of arched structures*. New York: Springer Science and Business Media 2012.

[4] Vanderplaat, G N. and Han, S H. Arch shape optimization using force approximation methods. *Structural Optimization*. 1990; **2**, 93-201. Springer Verlag.

[5] Heyman, J. Hooke's cubico-parabolical conoid. *Notes & Rec. Royal Soc*. 1998, **52**, 1, 39-50. (*doi*: 10.1098/rsnr.1998.0033).

[6] Lewis, W J. *Tension structures: form and behaviour*, 2nd Ed. London: ICE Publishing 2018.

[7] Tomlow, J. *The Model*. Publication of IL 1989; **34,** University of Stuttgart.

[8] Zerbst, A. *Antoni Gaudi*. Benedikt Taschen Verlag 1993; 110-115, English translation: Jones, D. & Gaines, J.

[9] Otto, F. and Rasch, B. *Finding form. Towards an architecture of the minimal*. Deutscher Werkbund Bayern. 1995. Edition Axel Menges.

[10] Michiels, T. and Adriaenssens, S. Form-finding algorithm for masonry arches subjected to in-plane earthquake loading, *Computers & Structures*. 2018; **195**, 85-98.

[11] Nodargi, N A. and Bisegna, P. Thrust line analysis revisited and applied to optimization of masonry arches, *International Journal of Mechanical Sciences*. 2020; **179**, 105690.

[12] Jorquera-Lucerga, J J. Form-finding of funicular geometries in spatial arch bridges through Simplified Force Density method. *Applied Sciences* 2008; **8**, 1-14.

[13] Cercadillo-Garcia, C. and Fernandez-Cabo JL. Analytical and numerical funicular analysis by means of parametric Force Density method. *Journal of Applied Research and Technology*. 2016; **14**, 108-124. (doi: 10.3390/app8122553).

[14] Wang, C Y and Wang C M. Closed-form solutions for funicular cables and arches. *Acta Mech.* 2015; **226**, 164-165 (doi 10.1007/s00707-014-1250-x).

[15] Oasys Software. GSA Version 10.1. Arup, 13 Fitzroy Street London W1T 4BQ, 2020.

[16] V Simulia, Dassault Systemes. "ABAQUS 6.13 User's manual." *Dassault Systems, Providence, RI* 305 (2013): 306.